JOURNAL OF GEOPHYSICAL RESEARCH, VOL. 115, D07302, doi:10.1029/2009JD012781, 2010

Click Here for Full Article

Multiscale carbon monoxide and aerosol correlations from satellite measurements and the GOCART model: Implication for emissions and atmospheric evolution

Huisheng Bian,[1,2] Mian Chin,[3] S. Randy Kawa,[3] Hongbin Yu,[1,2] Thomas Diehl,[1,2] and Tom Kucsera[1,2]

Received 2 July 2009; revised 23 October 2009; accepted 30 November 2009; published 8 April 2010.

[1] Regional correlations of CO and aerosol on different time scales provide information on their sources, lifetimes, and transport pathways. We examine regional and global column CO and fine-mode aerosol optical depth (AODf) correlations from daily to seasonal scales using 7 years (2000–2006) of satellite observations from the Measurement of Pollution in the Troposphere and the Moderate Resolution Imaging Spectroradiometer and model simulations from the Goddard Chemistry Aerosol Radiative Transport model. Our analyses indicate that, globally, column CO and AODf have similar spatial distributions due to their common source locations, although CO is more spatially dispersed because of its longer lifetime. However, temporal CO-AODf correlations differ substantially over different timescales and different regions. On daily to synoptic scales CO and AODf have a positive correlation over the industrial and biomass burning source regions owing to the covariance of emissions and coherent dynamic transport. No such correlation is seen in remote regions because of the diverging influence of mixing and chemical processes during longer-range transport. On the seasonal scale in the Northern Hemisphere, CO and AODf are out of phase by 2–4 months. This phase lag is caused by photochemical production of sulfate, which is the major component of fine-mode aerosol in the Northern Hemisphere, and photochemical destruction of CO in reaction with OH (both at maximum in the summer and at minimum in the winter), together with the seasonality of fine-mode dust, which peaks in the boreal spring season. In the Southern Hemisphere tropics and subtropics, however, CO and AODf are generally in-phase because the variability is dominated by direct release from biomass burning emissions.

Citation: Bian, H., M. Chin, S. R. Kawa, H. Yu, T. Diehl, and T. Kucsera (2010), Multiscale carbon monoxide and aerosol correlations from satellite measurements and the GOCART model: Implication for emissions and atmospheric evolution, *J. Geophys. Res.*, *115*, D07302, doi:10.1029/2009JD012781.

1. Introduction

[2] Atmospheric CO and aerosols share common characteristics, such as major sources (e.g., biomass burning, transportation, and industrial combustion) and dynamic transport, but differ in atmospheric chemistry and removal processes. Much effort has been made to understand their origins and atmospheric evolution by investigating their correlation for air quality studies. For example, CO and aerosols, which primarily originate from biomass burning and degrade local air quality, correlate strongly over a wide range of regions, from station sites [*Bremer et al.*, 2004; *Edwards et al.*, 2006], to regional areas [*Jones et al.*, 2001; *Massie et al.*, 2006; *DeCarlo et al.*, 2008, *Kleinman et al.*, 2008], to even the Southern Hemisphere (SH) as a whole [*Edwards et al.*, 2004]. Over industrial pollution regions, *Derwent et al.* [2001] observed the occurrence of large increases in black carbon aerosol concentrations that correlate well with similar increases in CO monitored near-simultaneously at the Mace Head Atmospheric Research Station on the Atlantic Ocean coast of Ireland, where polluted air masses come from the continent of Europe. Since CO shares a common major urban source with fine particles (aerosol particle diameter <1 μm), CO measurements have been used to derive fine aerosol number concentrations and emission factors on regional scales [*Longley et al.*, 2005].

[1]Goddard Earth Sciences and Technology Center, University of Maryland, Baltimore County, Baltimore, Maryland, USA.
[2]Also at Laboratory for Atmospheres, NASA Goddard Space Flight Center, Greenbelt, Maryland, USA.
[3]Laboratory for Atmospheres, NASA Goddard Space Flight Center, Greenbelt, Maryland, USA.

Copyright 2010 by the American Geophysical Union.
0148-0227/10/2009JD012781

However, on a hemispheric scale, atmospheric column CO and fine-mode aerosol seasonal cycles are out of phase by several months in the Northern Hemisphere (NH) zonal mean [*Edwards et al.*, 2004], which is primarily driven by the chemical process that removes CO in reaction with OH and the primary production of sulfate aerosols from the oxidation of SO_2 by OH. Although these studies have improved our understanding of atmospheric CO and aerosol evolution and distributions, they typically focus on either certain regions or certain time scales.

[3] Expanding on previous studies, here we examine the CO-aerosol correlation in different environments and on different time scales with both model simulations and various measurements (including those from satellites). We use the Goddard Chemistry Aerosol Radiative Transport (GOCART) model to understand and interpret the observed correlations between CO and fine-mode aerosol optical depth (AODf) from the Terra satellites on regional and global scales for daily, seasonal, and interannual variability from 2000 to 2006 (7 years). We further identify the determining factors for CO-AODf correlation using source and speciation information from GOCART tagged emission simulations.

[4] Based on the multiyear satellite data and model results, we address the following questions: (1) What is the CO-AODf correlation in different regions (industrial, tropical/subtropical biomass burning, polluted ocean, and remote ocean)? (2) How does the CO-AODf correlation change at different timescales (e.g., daily, seasonal, and annual)? and (3) How can CO-AODf relationships be explained in terms of sources (e.g., industrial or biomass burning), transport, and chemistry?

[5] In section 2 we describe GOCART CO and aerosol simulations, as well as various satellite and ground-based observations used in the model evaluation. Section 3 reports the evaluation of GOCART CO and aerosol simulations using various satellite and ground station measurements. In section 4 the satellite and model results are examined to identify the CO-AODf relationships and to discuss their relevance to pollutant emissions, chemistry, and transport over different spatial and temporal scales. Finally, the conclusions and implications of the study are summarized in section 5.

2. Description of Model Simulations and Measurements of Aerosol and CO

2.1. Goddard Chemistry Aerosol Radiative Transport (GOCART) Model

[6] The GOCART model, driven by assimilated meteorological fields from the Goddard Earth Observing System (GEOS) Data Assimilation System (DAS), version 4, simulates major aerosol types and CO. The spatial resolution of the GOCART model used in this study is 2° latitude by 2.5° longitude horizontally and 30 layers vertically.

2.1.1. CO Simulation

[7] CO simulation capability has recently been incorporated into the GOCART model on the basis of the study by *Bian et al.* [2007]. The CO module includes direct emissions from the burning of fossil fuel, biofuel, and biomass. CO anthropogenic emission was compiled for the year 2001 Transport and Atmospheric Chemistry Near the Equator-Pacific (TRACE-P) campaign, with the Asia emission replaced by the emission inventory of *Streets et al.* [2006]. The interannual change of CO follows the pattern of multi-year anthropogenic black carbon change that was provided by Streets et al. as well. The module also includes photochemical production as indirect emission from the coemitted nonmethane hydrocarbons from combustion and from biogenic sources. The chemical processes include production from CH_4 and loss via reactions with OH. In this study we use the biomass burning emission inventory from the Global Fire Emission Data Set version 2 (GFED2) [*van der Werf et al.*, 2006]. Unlike our previous CO study, in which the OH field was taken from the GEOS-CHEM model and the CH_4 field was taken from NOAA Global Monitoring Division (GMD) observations [*Bian et al.*, 2007], we adopt both the OH and the CH_4 fields from the Global Modeling Initiative (GMI) [*Duncan et al.*, 2008] generated by GEOS-4 meteorological fields, the same ones used in driving CO and aerosol transport in this study.

2.1.2. Aerosol Simulation

[8] Aerosol simulation in the GOCART model has been described in detail in previous studies [e.g., *Chin et al.*, 2000, 2002, 2007; *Ginoux et al.*, 2001, 2004]. Briefly, it includes the major aerosol types sulfate, dust, black carbon, organic carbon, and sea salt, and the precursor gas species sulfur dioxide (SO_2) and dimethyl sulfide (DMS). The model accounts for emissions from anthropogenic, biomass burning, biogenic, and volcanic sources, wind-blown dust, and sea salt. It also includes atmospheric processes of chemistry, convection, advection, boundary layer mixing, dry and wet deposition, and gravitational settling. Dry particle sizes and their hygroscopic growth with increasing relative humidity are prescribed based on Optical Properties of Aerosols and Clouds (OPAC) [*Hess et al.*, 1998; *Chin et al.*, 2002]. Anthropogenic, biomass burning, and volcanic emissions from 2000 to 2006 were updated recently [*Streets et al.*, 2006; *van der Werf et al.*, 2006]. Emission of SO_2 from sporadic and continuous volcano eruptions are reprocessed based on the Global Volcanism Program's database provided by the Smithsonian Institution, Total Ozone Mapping Spectrometer, and Ozone Monitoring Instrument SO_2 retrieval [*Chin et al.*, 2000].

[9] Fine-mode aerosol was used in the study because satellite measurements provide a fine-mode aerosol product and it is of primary interest for air quality. Anthropogenic and biomass burning aerosols, which share common sources with CO, account for the majority of fine-mode aerosol. GOCART fine-mode aerosol consists of simulated sulfate, black carbon, and organic carbon from both anthropogenic and natural sources. In addition, dust and sea-salt aerosol particles <1 μm in diameter are included as part of the fine-mode aerosol.

2.2. Measurements of CO and Aerosol

[10] The sensors on the EOS satellites have provided, for the first time, concurrent global measurements of CO and aerosols since 2000. There is also a suite of measurements from ground-based networks that are used to evaluate model simulations.

2.2.1. CO Measurements

[11] The Measurement of Pollution in the Troposphere (MOPITT) instrument on the EOS-Terra satellite has been

providing global measurements of CO in the middle-upper troposphere at a swath width of 640 km, covering the globe once about every 3–4 days. MOPITT is a nadir-viewing gas correlation radiometer and its retrieval depends on the thermal contrast between the surface and the atmosphere, which leads to little CO sensitivity in the boundary layer [*Deeter et al.*, 2003]. Like most passive remote measurements, MOPITT retrieval provides the averaging kernel matrix to record the relative vertical weighting of a particular measurement. The retrieval averaging kernels are dependent on the surface albedo, the surface-to-air temperature contrast, an a priori CO vertical profile (i.e., a preassumed background CO profile), and a covariance matrix of the uncertainty in the a priori CO profile [*Bian et al.*, 2007]. We use the level 3, 1° × 1° gridded, daily data in this study. The validation indicates that the biases of retrievals are 8–10 ppbv in the lower troposphere, 2–5 ppbv in the midtroposphere, and a slightly negative value in the upper troposphere and lower stratosphere over various regular aircraft measurement sites and a number of campaigns [*Emmons et al.*, 2004].

[12] We also use data from ground-based measurements to evaluate model and satellite data further and to assist in model analysis. The NOAA GMD Carbon Cycle Greenhouse Gases observational network (http://www.cmdl.noaa.gov/ccgg/index.html) has been providing long-term measurements of CO at a sampling frequency of approximately once per week at local noontime. Only data with an acceptable quality flag (i.e., a period in the first column of the quality control flags) [*Novelli et al.*, 1992] are used in our comparisons.

2.2.2. Aerosol Measurements

[13] The Moderate Resolution Imaging Spectroradiometer (MODIS) on the EOS-Terra satellite has been measuring the column AOD and fine-mode fraction since 2000. Its AODf is a fraction of the AOD contributed by the aerosol modes with an effective radius of <1.0 μm. MODIS aerosol retrieval uses separate algorithms over land and ocean to obtain aerosol optical properties in cloud-free areas, including AOD and AODf at 550 nm [e.g., *Kaufman et al.*, 1997; *Tanré et al.*, 1997; *Chu et al.*, 2003; *Remer et al.*, 2005; *Levy et al.*, 2007]. Over ocean, the algorithm combines lognormal modes. Over land, bilognormal models are used in the algorithm (C. R. Levy et al., Global evaluation of the collection 5 MODIS aerosol products over land and ocean, submitted to *Atmospheric Chemistry and Physics Discussions*, 2009). With a local equatorial overpass time of about 1030 and a 2300 km wide swath, the MODIS on Terra provides near-global coverage every 1 or 2 days. We use the most recent version (collection 5) of the level 3, quality-assured Terra MODIS monthly mean product, which is a globally gridded data set at 1° × 1° horizontal resolution. A recent evaluation of this data set demonstrated that the global expected uncertainty for spectral AODf (or τ) is $\pm(0.05 + 0.15\tau)$ and $\pm(0.04 + 0.05\tau)$ over dark land and ocean, respectively (Levy et al., submitted manuscript, 2009).

[14] The Aerosol Robotic Network (AERONET), an international federated Sun photometer network [*Holben et al.*, 1998], has ground-based remote-sensing monitoring stations covering virtually all aerosol regimes over a wide range of geographic locations. AERONET measures total column aerosol spectral optical depth with an accuracy of 0.01–0.02 [*Eck et al.*, 1999] at several visible and near-infrared wavelengths. Only data at 550 nm are used here. Like satellite sensors, the Sun photometer acquires aerosol data only during daylight under cloud-free conditions. We use the quality-assured and cloud-screened version 2, level 2, inversion product of fine-mode aerosol data [*Smirnov et al.*, 2000; *Dubovik et al.*, 2002; *Eck et al.*, 2008]. The current inversion data, based on the fine-mode/coarse-mode division at the minimum value of the (volume) particle size distribution, provide a slightly lesser fine-mode fraction than did the previous version, which had a purely mechanical cutoff at a radius of 0.6 μm [*O'Neill et al.*, 2008; available at http://aeronet.gsfc.nasa.gov/new_web/publications.html].

3. Comparisons of GOCART Simulation With Observations

[15] In this section we compare CO and AODf data simulated by GOCART with those retrieved from the remote sensing instruments and measured at the surface sites. For proper comparisons with MOPITT-retrieved CO data, model results have to be weighted vertically to take into account retrieval sensitivity at different altitudes, which is highest in the midtroposphere. We have adjusted the modeled CO data to make them "satellite equivalent" using the averaging kernel information [e.g., *Bian et al.*, 2007] that is provided with the MOPITT products.

3.1. Evaluation of the Model CO Simulation

[16] Figure 1 shows global distributions of the 500 hPa CO mixing ratio simulated by the GOCART model and retrieved by MOPITT during January and July 2006. GOCART CO shown in Figure 1 has been reprocessed with the MOPITT averaging kernel. It shows that the model captures MOPITT-observed CO distribution patterns well during the 2 months including high CO over industrial regions (East Asia, West Europe, and North America) and their downwind regions, high CO over biomass burning regions of West Africa, and a hemispheric CO gradient from higher in the north to lower in the south. However, the model CO is typically about 15%–20% lower in magnitude. We did several tests to identify the reasons for this. Among the testing parameters and/or processes, the OH field introduces a large change in the CO column. Global average CO is about 12% higher when using GEOS-CHEM OH instead of GMI OH. Global average CO is about another 8% higher when the simulations use the emission value of *Duncan et al.* [2008] instead of the GFED2 biomass burning emission. We used GMI OH and GFED2 biomass burning emissions in this study since they provided multiyear data that we needed.

[17] The seasonal variation of the model simulated surface CO mixing ratio from 2000 to 2006 is compared with the measurements at 41 GMD sites. Figure 2 shows the comparisons over six of these sites that represent different geographic regions (Arctic, midlatitude land, midlatitude ocean, and Antarctic) and pollutant environments (industrial polluted region, biomass-burning-dominated region, and remote region). The modeled CO is also shown according to its origins from different sources. The model generally captures the mean levels and the seasonality at all locations, with 15%–30% lower amplitudes than in observations at the

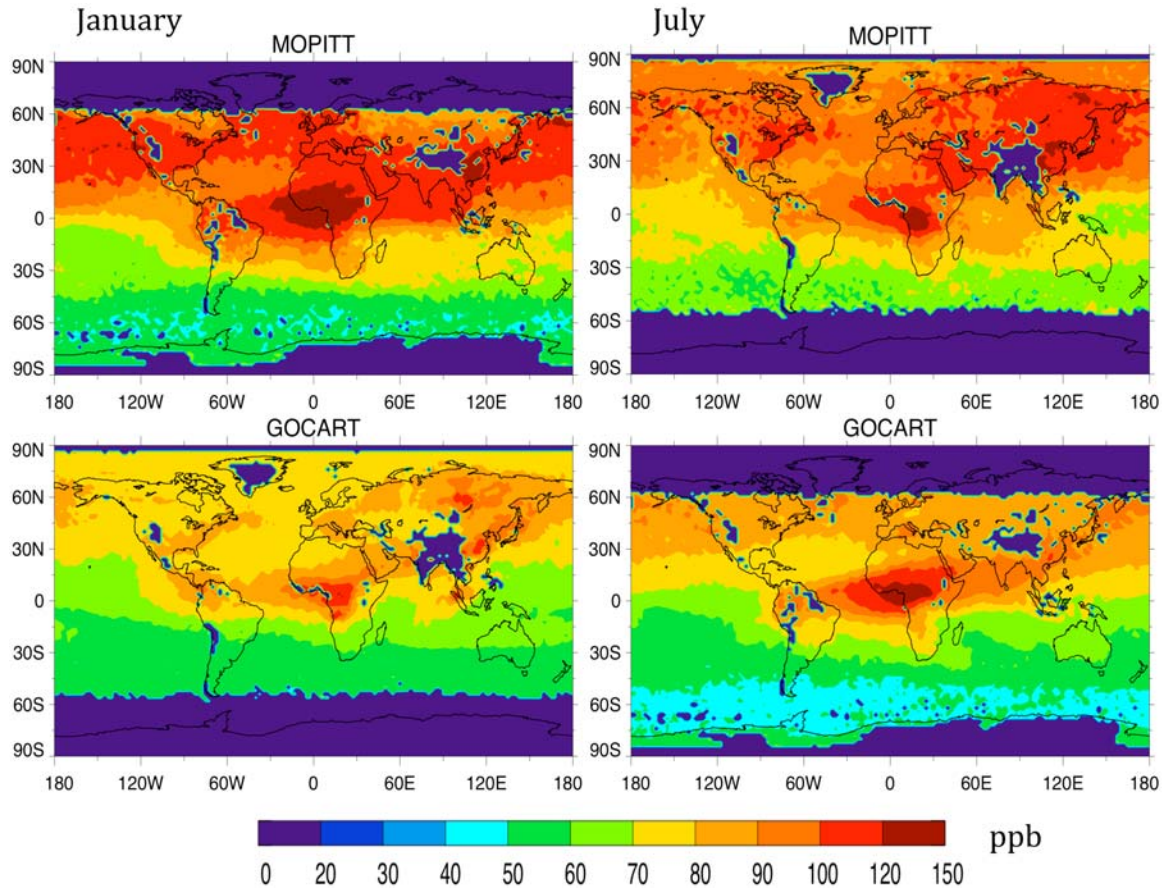

Figure 1. Monthly CO (in parts per billion) in 500 mb from (top) satellite Measurement of Pollution in the Troposphere (MOPPIT) and (bottom) Goddard Chemistry Aerosol Radiative Transport (GOCART) model in (left) January and (right) July 2006. GOCART CO reprocessed with MOPITT average kernel.

polar and remote oceanic stations Alert, Canada, Palmer Station, Antarctica, and Mauna Loa Observatory. These CO comparisons are consistent with the sensitivity tests in previous studies [*Bian et al.*, 2007].

3.2. Evaluation of the Model Aerosol

[18] Monthly global GOCART aerosol AODf at 550 nm is compared with MODIS retrievals for January and July 2006 in Figure 3. MODIS retrievals are missing over polar regions owing to low light signals and bright surfaces and over arid and semiarid regions owing to high surface reflection. The high MODIS AODf over the northern border of Russia in July is most likely due to retrieval uncertainties because there is no local biomass burning there. Generally speaking, the GOCART simulation captures the high AODf values observed by MODIS over the industrial sources and their downwind regions, biomass burning regions like central Africa in July, and downwind regions of deserts. However, the GOCART model gives consistently lower AODf values than MODIS does over tropical Pacific and SH remote oceans where sea salt dominates. MODIS retrieval over southern oceans may be contaminated by clouds and whitecaps [*Yu et al.*, 2003].

[19] Figure 4 shows a comparison of monthly AODf values at 550 nm from GOCART, MODIS, and AERONET at six representative AERONET sites during the 7 year period. Further indicated in Figure 4 is the contribution of each aerosol component to AODf by GOCART. Basically, the model underestimates the seasonal variations of AODf observed by MODIS and AERONET over all industrial and biomass burning stations. For example, during summer, the modeled AODf at GSFC in the polluted area of the eastern United States is typically lower than those of MODIS and AERONET by more than 30%. This low value may be caused by the excessive wet scavenging in the model over the eastern United States during summer [*Chin et al.*, 2000]. The Abracos Hill site in South America, which is strongly influenced by local seasonal biomass burning emission, shows dramatic interannual AODf variations; the model underestimates the peak AODf values there except for the 2 intensive biomass burning years of 2004 and 2005. The model fine-mode aerosol over Cape Verde, downwind of the Sahara Desert, agrees well with AERONET and MODIS measurements during boreal winter to spring, when the majority of fine- mode aerosols come from the Sahara, but the model AODf is higher than AEROENT and lower than MODIS values during boreal summer, when a considerable portion of the aerosols also comes from industrial and biomass burning emissions. Midway Island, located in the central north Pacific, has the lowest AODf among the six

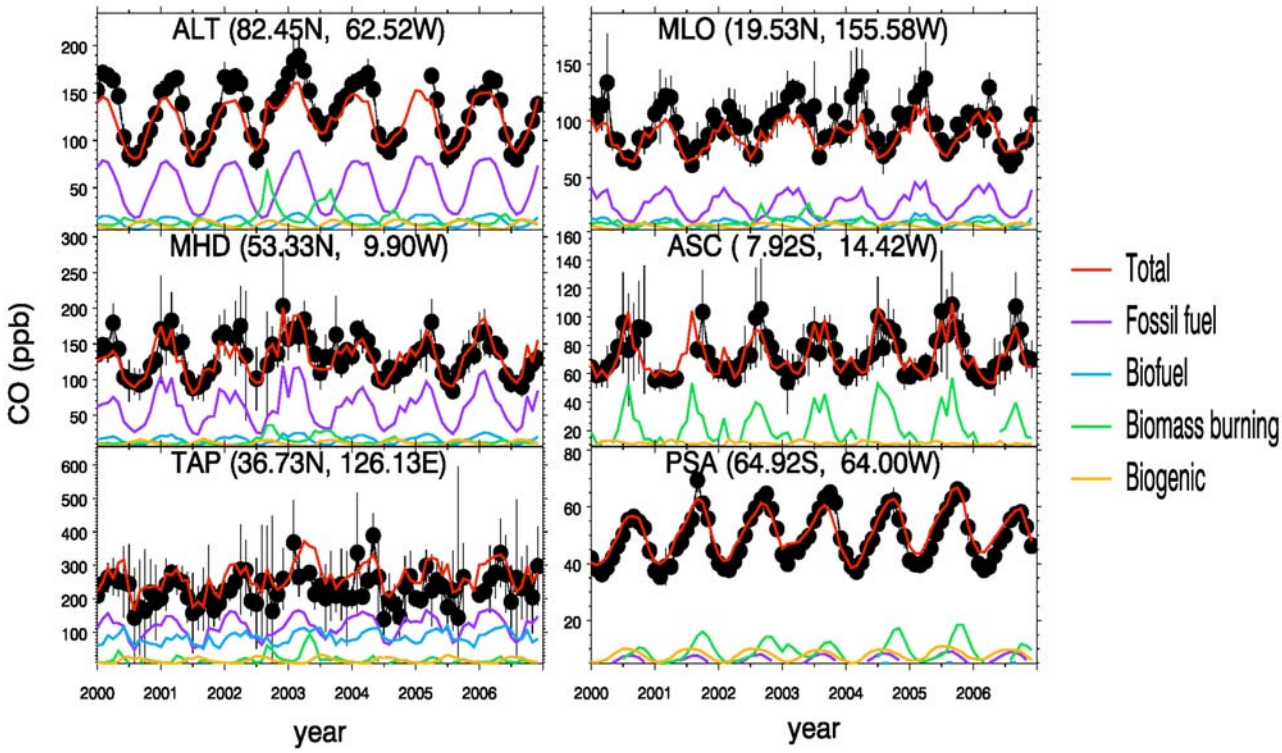

Figure 2. Seven-year surface station CO (in parts per billion) observations (black line with shaded circles) compared with GOCART model simulations (red line) over six GMD stations: ALT, Alert, Canada; ASC, Ascension Island, U.K.; MHD, Mace Head, Ireland; MLO, Mauna Loa, USA; PSA, Palmer Station, USA; TAP, Tae-ahn Peninsula, Korea. Colored lines represent model CO mixing ratios that come from different sources.

stations, and the model AODf level there agrees with those observed from MODIS but is higher than those observed from AERONET.

[20] The overall comparison of AODf among the model, MODIS, and AERONET at all AERONET sites, separated by land and ocean locations, is given in Figure 5. Relatively high correlations (>0.6) are obtained between modeled and AERONET AODf for both land and ocean sites. The model agrees with AERONET measurements better over ocean stations than over land stations. For example, the model mean AODf is closer to the ocean's AERONET mean AODf (i.e., the relative bias, B, is 0.86 over land and 1.01 over ocean) and the root mean square error is lower for ocean stations (0.09) than for land (0.12). A similar conclusion can be derived from the comparison between MODIS satellite measurements and AERONET ground station measurements. Our evaluation supports previous findings that the MODIS fine-mode fraction has larger uncertainties over land than over ocean [*Kleidman et al.*, 2005; Levy et al., submitted manuscript, 2009].

4. Relationship Between CO and Fine-Mode Aerosol Optical Depth (AODf)

4.1. Zonal Mean CO-AODf Correlation

[21] We analyze CO-AODf correlations over various atmospheric regions and time scales. First, we look at the overall global zonal mean column CO-AODf relationship observed by MOPITT and MODIS satellites and simulated by the GOCART model from the beginning of 2003 to the end of 2006, as shown in Figure 6. Note that the areas without MODIS retrieval, such as the Sahara Desert and the Arabian Peninsula, are excluded in the sampling of model zonal mean AODf calculation. Similarly, the areas without MOPITT retrieval, owing to cloud cover or high mountains, are also excluded in the sampling of model zonal mean CO calculation. The monthly zonal means from the model are calculated from the daily mean values that are not coincident with the satellite measurements.

[22] Although both MOPITT column CO and MODIS AODf are high over NH midlatitudes and tropical regions in certain months, their spatial and temporal patterns are different. Spatially, AODf is located closer to source regions, while column CO spreads more widely, particularly to high latitudes. In addition, there is a clear column CO tilt in the NH from around the subtropical regions in boreal winter season to about 60°N in the spring season, but the AODf distribution does not show such a pattern. All of these phenomena are attributed to the much longer lifetime of CO (weeks to months) compared to aerosols (days), which allows CO transport to reach more distant regions.

[23] Temporally, the maximum column CO over NH midlatitudes occurs several months ahead of the maximum AODf, while the maximum CO over SH tropical regions occurs at similar times as the maximum AODf. These temporal correlations imply information on pollutant emis-

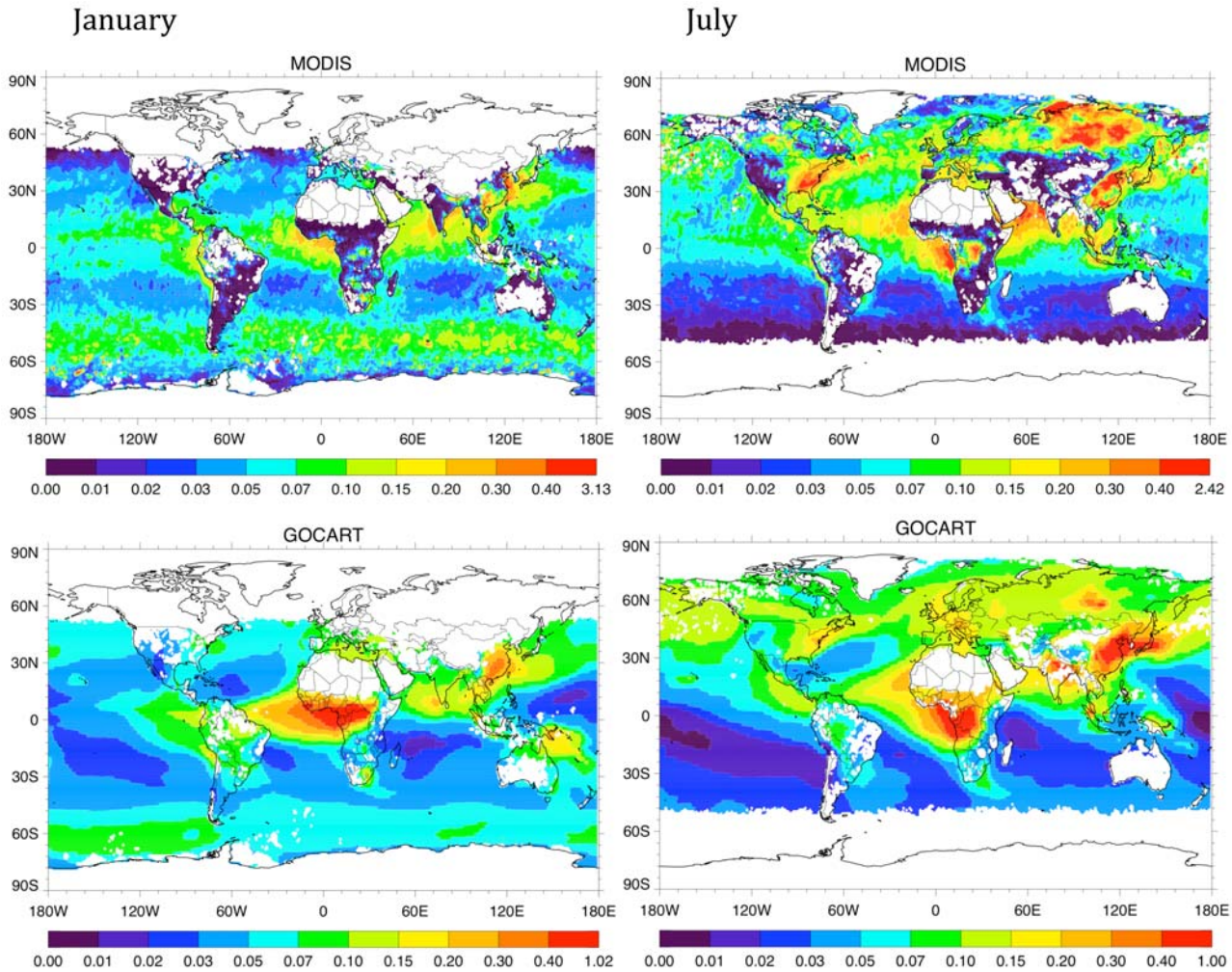

Figure 3. Comparison of monthly satellite (top) Moderate Resolution Imaging Spectroradiometer (MODIS) and (bottom) GOCART model fine-mode atmospheric optical depth (AODf) in 550 nm for (left) January and (right) July 2006. GOCART AODf sampled using the MODIS AODf spatial distribution.

sions, chemistry, and transport and are explained below by combining information on tagged CO sources and aerosol components provided by GOCART.

[24] In some regions the distributions of column CO and AODf differ substantially. For example, over the SH storm track, the seasonal high CO, transported from SH subtropical regions, occurs around August to October, while the seasonal high AODf, attributed to chemical sulfate production from local DMS emission, occurs around October to February. Zonal mean CO-AODf spatial and temporal relationships similar to those shown in satellite measurements are observed in GOCART simulations, although tracer levels do not entirely match between satellite and model data.

[25] The model-MODIS AODf comparison over tropical regions is particularly complex. There are several major fine-mode aerosol components within the tropical belt, such as fine-mode sea salt over tropical oceans, fine-mode dust from the deserts of the Sahara and the Arabian Peninsula, and biomass burning. Aerosols from burning peak in the Sahel during December–February, peak in southern Africa during June–July (first peak) and September–November (second and normally more intensive peak), peak in northern South America and Central America during February–March, and peak in Indonesia during March–June and August–November. Therefore, it is necessary to break the comparison down further over different regions within the tropical zonal belt to trace aerosol origins.

[26] Overall, the zonal mean GOCART column CO is 15%–20% lower than that of MOPITT (note that we use a different scale for MOPITT and GOCART CO in Figure 6), similar to the analysis in section 3.1.

4.2. CO-AODf Correlations on Daily to Synoptic Scales

[27] Although Figure 6 provides an overall CO-AODf relationship on a global zonal mean basis, the correlation is sometimes obscure owing to convoluted information from various regions with CO from different source types. In this section we further examine CO-AODf correlations over different source regions (e.g., anthropogenic or biomass burning) and on daily (synoptic), seasonal, and annual

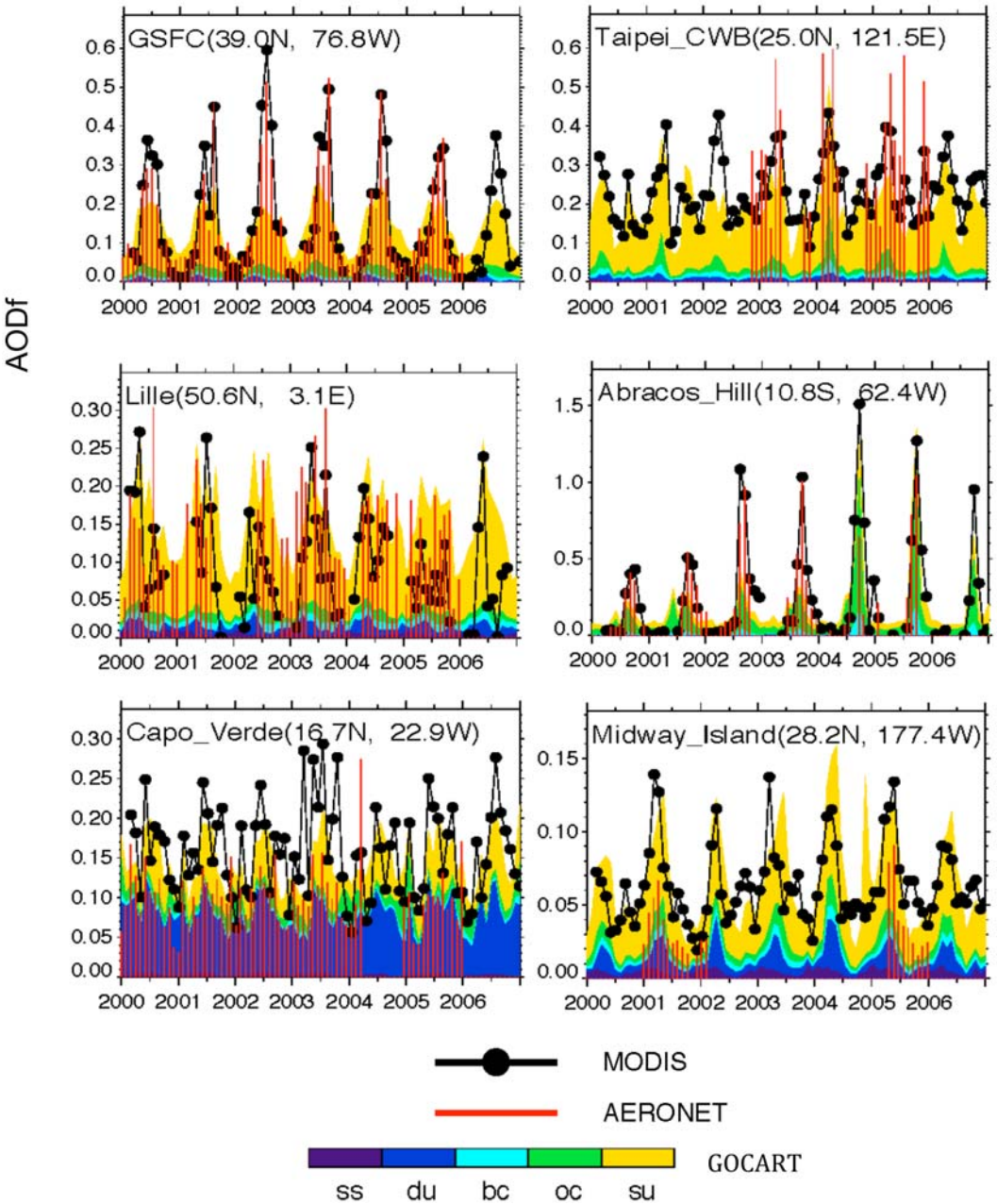

Figure 4. Comparison of 7 year monthly AODf (550 nm) from MODIS (solid black line with shaded circles), Aerosol Robotic Network (AERONET; red line), and GOCART model (colored areas tagged to different aerosol compositions) at six AERONET sites.

scales using the 7 years of GOCART simulation results. We also view CO-AODf relationships with the assistance of GOCART CO tagged to its source types and aerosol tagged to its components; such information can only be obtained from the model.

[28] Figure 7 shows the daily synoptic CO-AODf relationship in 2001 over the eastern United States (EUS; an NH industrial region), southern America (SAM; a biomass burning region), and the North Pacific (NPC; a remote NH oceanic region). Correlation coefficients (R_{hpass}) between daily AODf and column CO over the regions were calculated using a high-pass filter that eliminates changes with a time scale longer than 30 days. In source regions (EUS and SAM), CO and aerosol show a close synoptic-scale positive correlation, that is, R_{hpass} is 0.66 for EUS and 0.77 for SAM, whose variability is mainly determined by emission and daily synoptic atmospheric dynamic transport (e.g., mesoscale fronts). Dry and wet scavenging and OH chemical oxidation do not contribute to this daily synoptic covariability, since scavenging affects only aerosol particles, while chemistry is a source of fine-mode aerosol but a sink of CO.

[29] The column CO amount varies differently relative to AODf in several temporal segments in the EUS, while the two levels follow each other closely throughout the entire

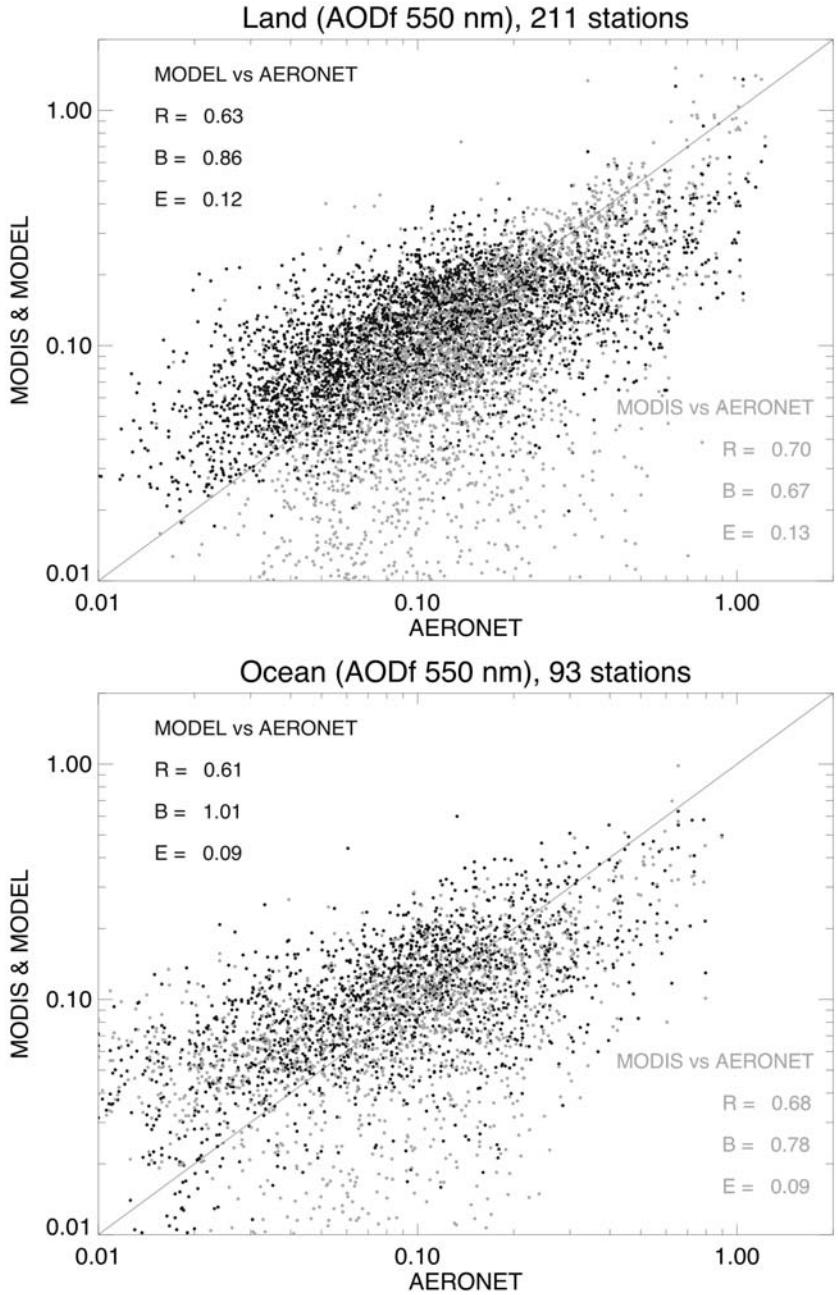

Figure 5. (top) Scatterplot of monthly mean AODf between AERONET observations over 211 ground land stations and GOCART simulations extracted at the corresponding AERONET sites during the years 2001–2006 (black circles) and between AERONET and satellite MODIS observation (gray circles). *R* is the correlation coefficient, *B* is the ratio of mean AODf of model (or MODIS) to that of AERONET, and *E* is the root mean square error. (bottom) Similar scatterplot for 93 AERONET ocean stations.

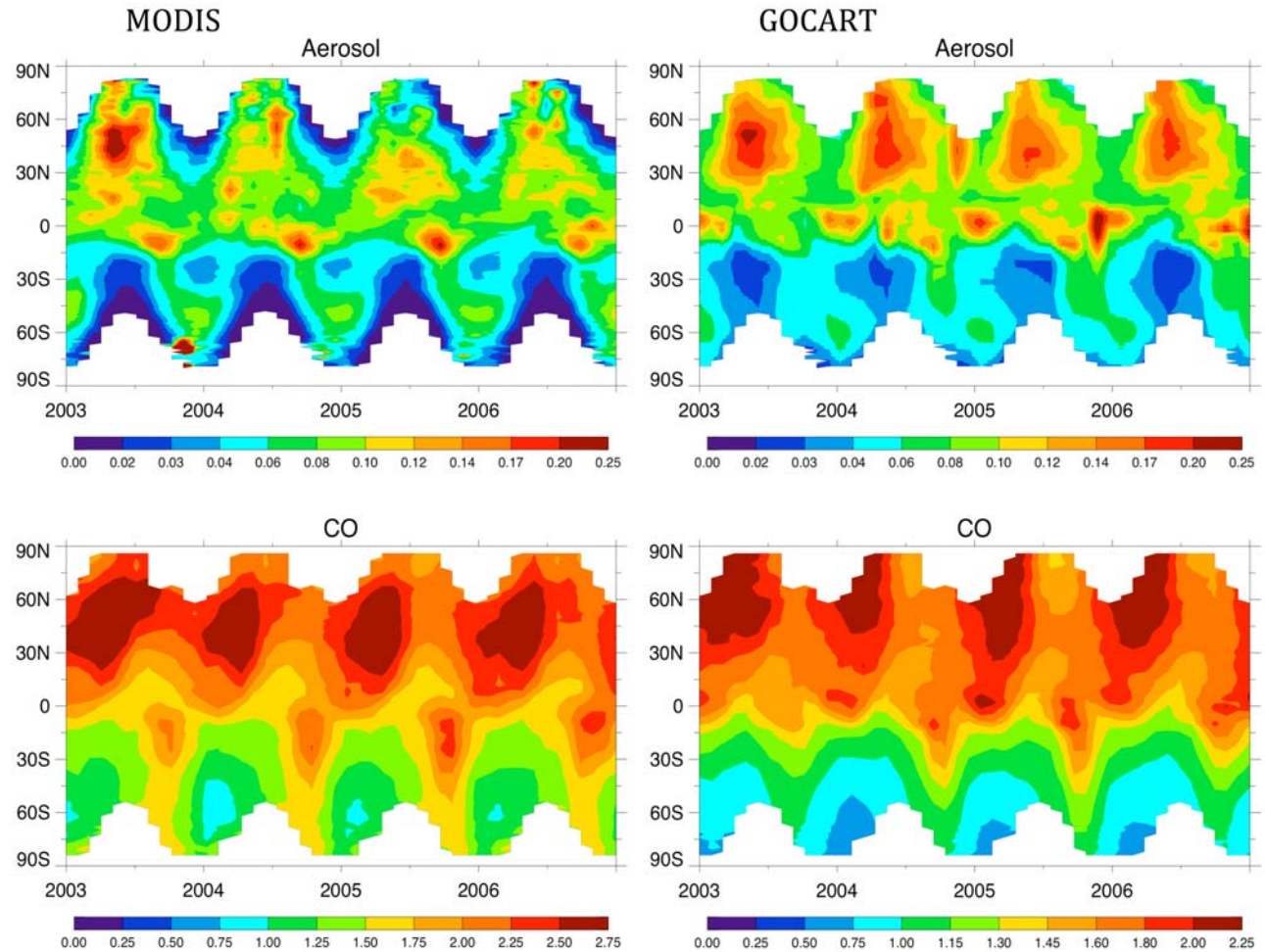

Figure 6. Global zonal mean monthly (top) AODf and (bottom) column CO (10^{18} molecules/cm^2) from (left) satellite observations and (right) model simulations for the years 2003–2006. Sample model data with satellite data spatially.

year in SAM. These seasonal features can be explained by the emission-tagged CO and aerosol components over the two regions (see discussion in the next section).

[30] A positive synoptic CO-AODf correlation, however, is not evident over the NPC (e.g., Figure 7, bottom), where R_{hpass} is only about 0.24, and the change pattern of CO sometimes appears to be anticorrelated with AODf. This is because CO over the NPC is produced by background CH_4 oxidation (almost flat over a synoptic scale) and comes from the long-term transport of CO from various land source regions and emission types. Short-term CO variations, produced near source regions, are greatly attenuated by dynamic mixing during long-range transport. Unlike CO, AODf has local oceanic sources (i.e., SO_4 produced from DMS oxidation and fine-mode sea salt), which show obvious greater synoptic variation. In addition, since aerosol's lifetime is much shorter than CO's, the fraction of aerosol transported to the NPC is much smaller than that of CO.

4.3. CO-AODf Correlations on Seasonal and Annual Scales

[31] Seasonal variations of column CO and AODf observed from MOPITT and MODIS and simulated from GOCART (note that CO was reprocessed with the MOPITT kernel profile and a priori profile) over the NH, the SH, and the same three regions (EUS, SAM, and NPC) during 2000–2006 are shown in Figure 8. Also shown in Figure 8 are the correlation coefficients (R) of AODf between MODIS and GOCART and of column CO between MOPITT and GOCART over each region. The high calculated R(MODIS-GOCART) and R(MOPITT-GOCART) over all the regions imply that the model captures the observed CO and aerosol variations, lending confidence in use of the model to analyze the AODf and CO correlations.

[32] Clearly, over NH regions, AODf and column CO are out of phase, with the maximum and minimum CO values appearing several months earlier than those of AODf. Column CO and AODf are closely in-phase over the SH mean. The correlation of AODf and CO varies dramatically over different regions. The highest correlation coefficient is for SAM ($R(\mathrm{CO/AODf})_{\mathrm{go}} = 0.85$ and $R(\mathrm{CO/AODf})_{\mathrm{sat}} = 0.90$) and the lowest is for the NH ($R = 0.0$ and 0.17) and EUS ($R = 0.28$ and -0.12).

[33] To analyze the temporal relationship of the variations of CO versus AODf quantitatively, we calculate the correlation coefficient (R_{lag}) using the mean data and shift-

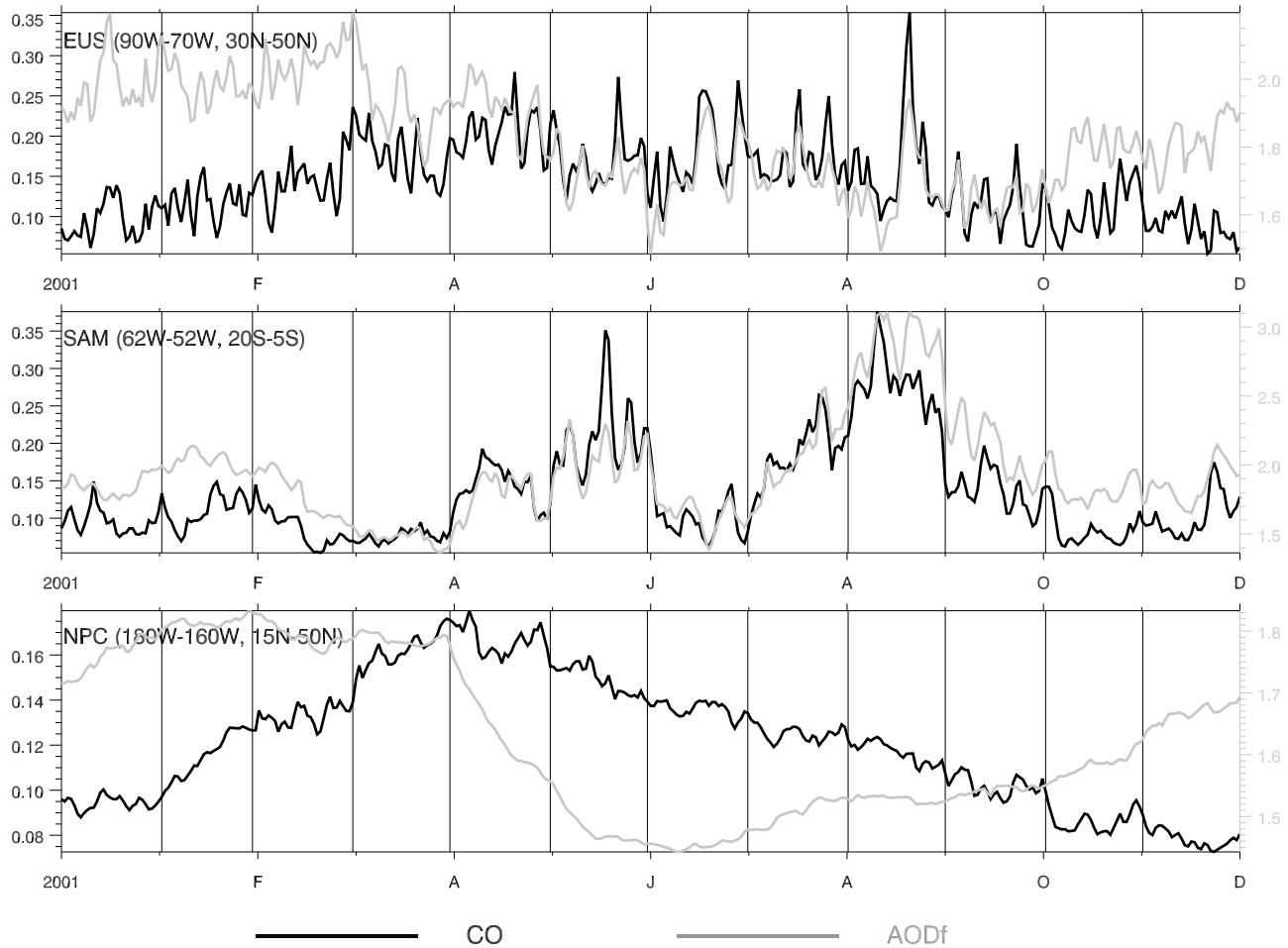

Figure 7. Daily variations of aerosol AODf and column CO (10^{18} molecules/cm^2) in the year 2001 over three regions: pollution region of eastern United States (EUS), biomass burning region of South America (SAM), and remote oceanic region of North Pacific (NPC).

ing the CO value at lags of 0 to 4 months (Figure 9) for the five regions. As shown above, the EUS, dominated by industrial sources, has the largest CO and AODf phase displacement (lag of ~3 months), while the SAM region, dominated by biomass burning emission, shows the same seasonality of CO and AODf (no lag of CO). The R_{lag} over the entire NH generally follows the pattern for the EUS, while that over the entire SH is compounded by imprints from biomass burning, industrial, and natural origins. The NPC has a relatively flat peak of R_{lag} between 1 and 3 months, which implies insensibility of remote ocean fields to the land industrial sources. In addition, the shape of the R_{lag} change along the x axis reflects the variability of CO and AODf amplitudes during their peak period in Figure 8 (and Figure 10). For example, SAM shows the sharpest CO and aerosol peak and, correspondingly, R_{lag} there has the largest change when shifting the CO phase.

[34] Why are seasonal CO and AODf cycles out of phase in NH regions but in phase in SH regions? If the out-of-phase CO-AODf relationship in polluted regions is controlled by OH (and H_2O_2) loss/production chemistry, then why are they not completely out of phase (i.e., by 6 months) but, instead, just shifted 2–4 months? To answer these questions, the seasonal variation of CO and aerosol and their source-tagged components over the same five regions during 2000–2006 are shown in Figure 10. Over NH regions (NH, EUS, and NPC), the fossil-fuel-related CO determines the regional column CO seasonal change, with seasonal highs during winter and early spring and seasonal lows during summer (the fossil fuel CO seasonal variation overshadows the opposing CO change associated with the biogenic source in Figure 10). This seasonality of fossil fuel CO is primarily determined by the photochemical loss of CO to OH oxidation, which is lowest during winter and highest during summer (note that the oxidant fields and reaction rates both have the pattern of a winter low and a summer high). This seasonality is intensified by the fossil fuel CO emission, which is 8% higher than the annual mean during winter and 8% lower during summer within tropical and subtropical regions (latitudes less than 30°), to account for the combustion engine efficiency, which varies with temperature [*Bian et al.*, 2007]. The aerosol components that determine the AODf seasonal change over NH regions are sulfate and, to a lesser extent, dust (Figure 10, right). Note that more than 95% of sulfate is not directly emitted but, rather, is photochemically produced by oxidation of SO_2 with OH in the gas phase and H_2O_2 in the aqueous phase (cloud or rain), both of which are also highest during

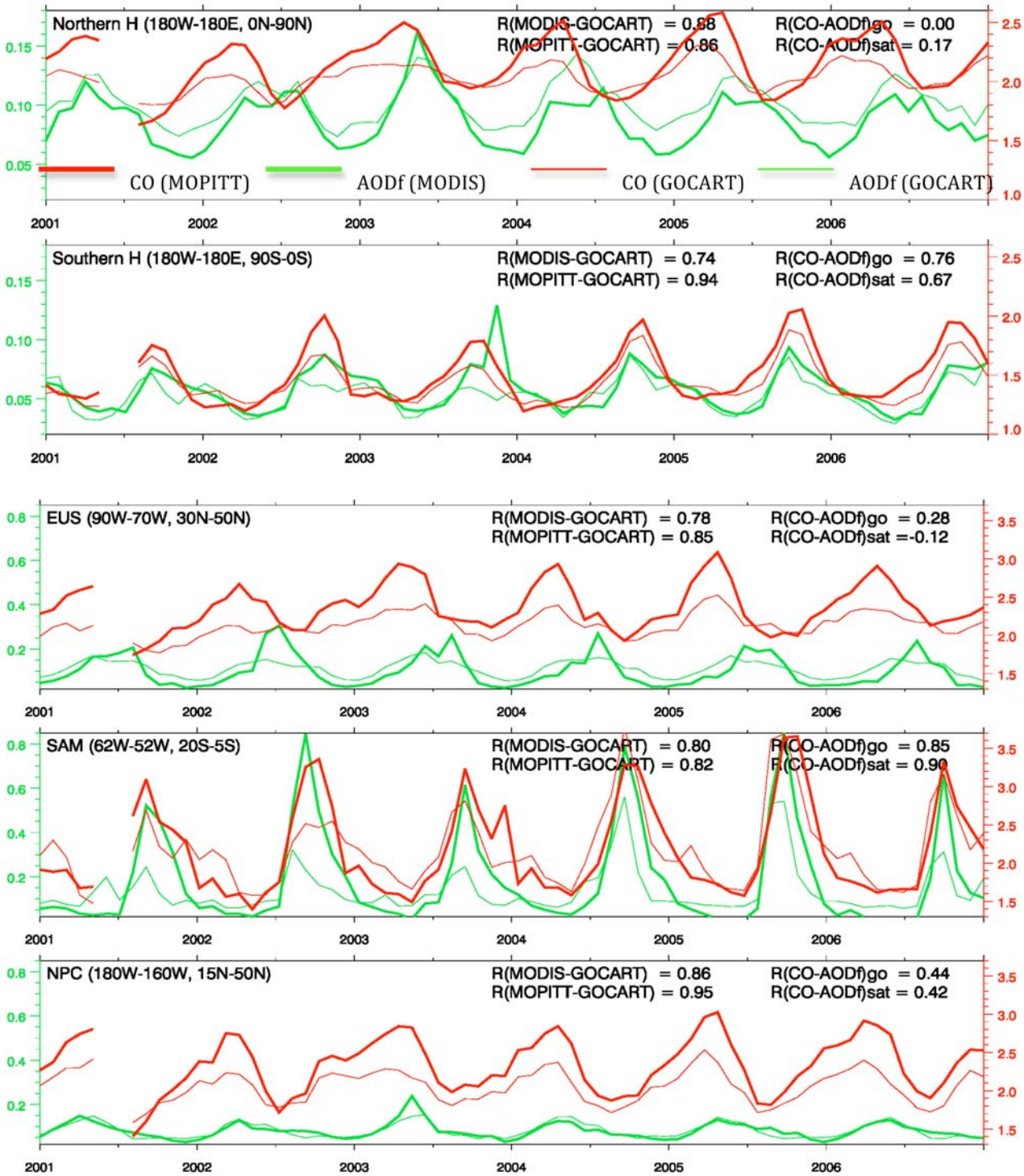

Figure 8. Monthly mean AODf (bold red line, MODIS; red line, GOCART) and column CO (10^{18} molecules/cm^2; bold green line, MOPITT; green line, GOCART) during the years 2001–2006 over the Northern Hemisphere (NH), Southern Hemisphere (SH), EUS, SAM, and NPC. High correlation coefficients between satellite measurement and model simulation for both AODf (*R*(MODIS/GOCART)) and column CO (*R*(MOPITT/GOCART)) calculated over all regions. Correlation between AODf and column CO from satellite observations (*R*(CO/AODf)sat) and from model simulations (*R*(CO/AODf)go) significantly different over regions.

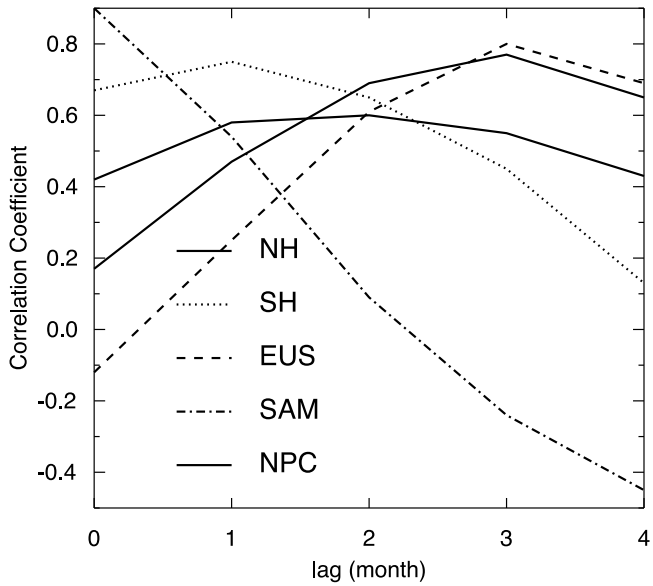

Figure 9. Correlation coefficients (R_{lag}) between monthly mean AODf and monthly mean CO over NH, SH, and three regions indicated in Figures 7 and 8 (EUS, SAM, and NPC). Lag of CO in calculation of correlation coefficients shown on the *x* axis.

summer and lowest during winter. NH SO_2 is mainly emitted from fossil fuel directly, constantly throughout the year except in Europe, where a seasonal variation is imposed, with a 30% higher-than-annual mean in winter and 30% lower-than-annual mean in summer in our model [*Chin et al.*, 2000]. In addition, we note that the highest total AODf shifts from summer to spring owing to the contribution of fine-mode dust (Figure 10, right). In summary, the different photochemical behaviors of CO (loss to OH) and aerosol (produced by OH and H_2O_2) over NH regions, along with regulation by other processes such as emission, deposition, and transport, result in the different seasonal variations of CO and aerosol there.

[35] On the contrary, over SAM, the seasonality of both column CO and AODf (mainly carbonaceous aerosols of black carbon and organic carbon; Figure 10, right) is determined by components originating from biomass burning sources. Unlike fossil fuel sources, emission from biomass burning has a pronounced seasonality and emits directly not only CO but also carbonaceous aerosols. Hence, a close seasonal correlation of CO and AODf results over SAM. There are two peaks of both column CO and AODf over SH. The first occurs during late austral winter and early spring, and the latter occurs during austral summer. The first peak is generated by biomass burning over SAM and southern Africa. The latter peak involves the biomass burning contribution that occurs over the Sahel during austral summer, the seasonal high of organic carbon from terpene emission, and the photochemical production of sulfate aerosol from ocean emissions of DMS.

[36] Also shown in Figure 10 is the annual average of CO and AODf over the NH and SH. Column CO and AODf both show year-to-year changes, which depend mainly on the change in emissions, particularly fossil fuel and biomass burning emissions. Although 7 years is not long enough to deduce robust trends, a general increase in both total CO and total AODf over both hemispheres is shown in our simulations.

[37] Our study confirms the seasonal correlation obtained from observational analyses by *Edwards et al.* [2004]. Our study has expanded their study (and other previous studies) by introducing model simulations tagged to each CO emission type and aerosol component to better explain the correlations quantitatively. Furthermore, we explore the correlation at the synoptic scale, where the correlation shows a pattern completely different from that at the seasonal and interannual scales.

5. Conclusions

[38] We have examined the spatial and temporal relationships between column CO and AODf using satellite (MOPITT and MODIS) measurements and GOCART model simulations. In particular, we have employed modeled CO and aerosol speciation to understand quantitatively the temporal variation of CO sources and aerosol components and to determine which atmospheric processes determine the relationship at various atmospheric regions and time scales. Therefore, our work has implications for air quality studies.

[39] Our results indicate that column CO and AODf have similar spatial distributions, both high over industrial- and biomass-burning-dominated regions, although AODf is more concentrated near the source regions owing to its shorter lifetime. This is because CO and fine-mode aerosols have many common emission sources, mainly from fossil fuel combustion and biomass burning. However, temporal CO-AODf relationships over different timescales can be very diverse. They have a strong positive correlation on the synoptic scale over industrial and biomass burning regions. However, the mixing process and the different emission, scavenging, and chemistry of CO and aerosols complicate and reduce their correlation over remote oceans. Their seasonal cycles can be either very similar or very different, depending on the source origins, that is, generally 2–4 months out of phase in the NH but in-phase in the SH. There are also year-to-year variations of CO and aerosol on regional and global scales, mostly controlled by emission, although the 7 year period is probably too short to derive meaningful trends.

[40] These findings are consistent with our understanding of sources, chemistry, and transport of CO and aerosols. The common sources of CO and aerosols from industrial and biomass burning emissions enable the tracers to have similar spatial distributions over the majority of land and nearby ocean regions. Dynamic transport over the source regions forces the tracers to be subject to the same atmospheric movement, so that a high positive correlation over synoptic scales is found between the tracers. Correlation of the CO-AODf seasonal cycles is controlled by both emission and chemistry. Over the NH, where anthropogenic emission dominates and the emissions are year-round, CO-AODf is out of phase because of the photochemical reactions that present a sink of CO but, at the same time, a source of sulfate aerosols (which accounts for most of the pollutant aerosols in the NH). Over the SH, where biomass burning dominates, CO-AODf is in-phase because biomass burning

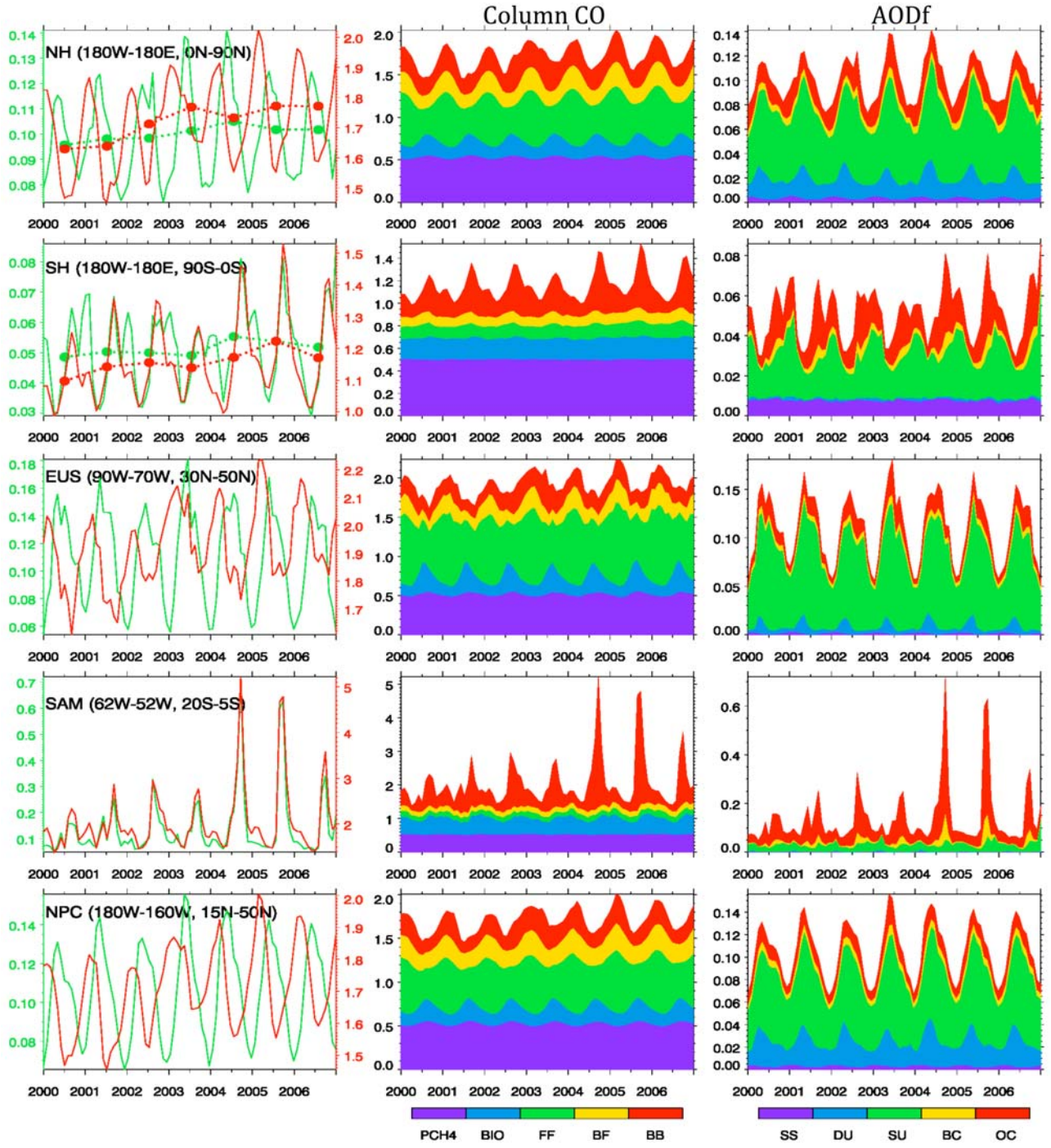

Figure 10. (left) GOCART monthly mean AODf and column CO (10^{18} molecues/cm^2) over NH, SH, EUS, SAM, and NPC during the years 2000–2006. Interannual variations of aerosol AODf (green line) and column CO (red line) for NH and SH also shown. (middle) Column CO tagged to different CO sources. (right) AODf tagged to different aerosol components.

directly emits not only CO, but also aerosols (i.e., the dominated carbonaceous aerosols).

References

Bian, H., M. Chin, R. Kawa, B. Duncan, A. Arellano Jr., and R. Kasibhatla (2007), Uncertainty of global CO simulations constraint by biomass burning emissions, *J. Geophys. Res.*, *112*, D23308, doi:10.1029/2006JD008376.

Bremer, H., J. Kar, J. R. Drummond, F. Nichitu, J. Zou, and J. Liu (2004), Spatial and temporal variation of MOPITT CO in Africa and South America: A comparison with SHADOZ ozone and MODIS aerosol, *J. Geophys. Res.*, *109*, D12304, doi:10.1029/2003JD004234.

Chin, M., R. B. Rood, S.-J. Lin, J.-F. Müller, and A. M. Thompson (2000), Atmospheric sulfur cycle simulated in the global model GOCART: Model description and global properties, *J. Geophys. Res.*, *105*, 24,671–24,687, doi:10.1029/2000JD900384.

Chin, M., P. Ginoux, S. Kinne, O. Torres, B. N. Holben, B. N. Duncan, R. V. Martin, J. A. Logan, A. Higurashi, and T. Nakajima (2002), Tropospheric

aerosol optical thickness from the GOCART model and comparisons with satellite and Sun photometer measurements, *J. Atmos. Sci.*, *59*, 461–483, doi:10.1175/1520-0469(2002)059<0461:TAOTFT>2.0.CO;2.

Chin, M., T. Diehl, P. Ginoux, and W. Malm (2007), Intercontinental transport of pollution and dust aerosols: Implications for regional air quality, *Atmos. Chem. Phys.*, *7*, 5501–5517.

Chu, D. A., Y. J. Kaufman, G. Zibordi, J. D. Chern, J. Mao, C. Li, and B. N. Holben (2003), Global monitoring of air pollution over land from EOS-Terra MODIS, *J. Geophys. Res.*, *108*(D21), 4661, doi:10.1029/2002JD003179.

DeCarlo, P. F., et al. (2008), Fast airborne aerosol size and chemistry measurements above Mexico City and central Mexico during the MILAGRO campaign, *Atmos. Chem. Phys.*, *8*(D21), 4027–4028.

Deeter, M. N., et al. (2003), Operational carbon monoxide retrieval algorithm and selected results for the MOPITT instrument, *J. Geophys. Res.*, *108*(D14), 4399, doi:10.1029/2002JD003186.

Derwent, R. G., D. B. Ryall, S. G. Jennings, T. G. Spain, and P. G. Simmonds (2001), Black carbon aerosol and carbon monoxide in European regionally polluted air masses at Mace Head, Ireland, during 1995–1998, *Atmos. Environ.*, *35*, 6371–6378, doi:10.1016/S1352-2310(01)00394-6.

Dubovik, O., B. Holben, T. F. Eck, A. Smirnov, Y. J. Kaufman, M. D. King, D. Tanre, and I. Slutsker (2002), Variability of absorption and optical properties of key aerosol types observed in worldwide locations, *J. Atmos. Sci.*, *59*, 590–608, doi:10.1175/1520-0469(2002)059<0590:VOAAOP>2.0.CO;2.

Duncan, B. N., J. J. West, Y. Yoshida, A. M. Fiore, and J. R. Ziemke (2008), The influence of European pollution on ozone in the Near East and northern Africa, *Atmos. Chem. Phys.*, *8*, 2267–2283.

Eck, T. F., B. N. Holben, J. S. Reid, O. Dubovik, A. Smirnov, N. T. O'Neill, I. Slutsker, and S. Kinne (1999), Wavelength dependence of the optical depth of biomass burning, urban, and desert dust aerosol, *J. Geophys. Res.*, *104*, 31,333–31,350, doi:10.1029/1999JD900923.

Eck, T. F., et al. (2008), Spatial and temporal variability of column-integrated aerosol optical properties in the southern Arabian Gulf and United Arab Emirates in summer, *J. Geophys. Res.*, *113*, D01204, doi:10.1029/2007JD008944.

Edwards, D. P., et al. (2004), Observations of carbon monoxide and aerosols from the Terra satellite: Northern Hemisphere variability, *J. Geophys. Res.*, *109*, D24202, doi:10.1029/2004JD004727.

Edwards, D. P., et al. (2006), Satellite-observed pollution from Southern Hemisphere biomass burning, *J. Geophys. Res.*, *111*, D14312, doi:10.1029/2005JD006655.

Emmons, L. K., et al. (2004), Validation of MOPITT CO retrievals with aircraft in situ profiles, *J. Geophys. Res.*, *109*, D03309, doi:10.1029/2003JD004101.

Ginoux, P., M. Chin, I. Tegen, J. Prospero, B. Holben, O. Dubovik, and S.-J. Lin (2001), Sources and distributions of dust aerosols simulated with the GOCART model, *J. Geophys. Res.*, *106*, 20,225–20,273, doi:10.1029/2000JD000053.

Ginoux, P., J. Prospero, O. Torres, and M. Chin (2004), Long-term simulation of dust distribution with the GOCART model: Correlation with the North Atlantic oscillation, *Environ. Model. Softw.*, *19*, 113–128, doi:10.1016/S1364-8152(03)00114-2.

Hess, M., P. Köpke, and I. Schult (1998), Optical Properties of Aerosols and Clouds: The software package OPAC, *Bull. Am. Meteorol. Soc.*, *79*(5), 831–844, doi:10.1175/1520-0477(1998)079<0831:OPOAAC>2.0.CO;2.

Holben, B. N., et al. (1998), AERONET—A federated instrument network and data archive for aerosol characterization, *Remote Sens. Environ.*, *66*, 1–16, doi:10.1016/S0034-4257(98)00031-5.

Jones, N. B., C. P. Rinsland, L. J. Ben, and J. Rosen (2001), Correlation of aerosol and carbon monoxide at 45°S: Evidence of biomass burning emissions, *Geophys. Res. Lett.*, *28*, 709–712, doi:10.1029/2000GL012203.

Kaufman, Y. J., D. Tanre, L. A. Remer, E. F. Vermote, A. Chu, and B. N. Holben (1997), Operational remote sensing of tropospheric aerosol over land from EOS moderate resolution imaging spectroradiometer, *J. Geophys. Res.*, *102*, 17,051–17,067, doi:10.1029/96JD03988.

Kleidman, R. G., N. T. O'Neill, L. A. Remer, Y. J. Kaufman, T. F. Eck, D. Tanré, O. Dubovik, and B. N. Holben (2005), Comparison of Moderate Resolution Imaging Spectroradiometer (MODIS) and Aerosol Robotic Network (AERONET) remote-sensing retrievals of aerosol fine mode fraction over ocean, *J. Geophys. Res.*, *110*, D22205, doi:10.1029/2005JD005760.

Kleinman, L. I., et al. (2008), The time evolution of aerosol composition over the Mexico City plateau, *Atmos. Chem. Phys.*, *8*, 1559–1575.

Levy, R. C., L. Remer, S. Mattoo, E. Vermote, and Y. J. Kaufman (2007), Second-generation algorithm for retrieving aerosol properties over land from MODIS spectral reflectance, *J. Geophys. Res.*, *112*, D13211, doi:10.1029/2006JD007811.

Longley, I. D., D. W. F. Inglis, M. W. Gallagher, P. I. Williams, J. D. Allan, and H. Coe (2005), Using NO_x and CO monitoring data to indicate fine aerosol number concentrations and emission factors in three UK conurbations, *Atmos. Environ.*, *39*, 5157–5169, doi:10.1016/j.atmosenv.2005.05.017.

Massie, S. T., J. C. Gille, D. P. Edwards, and S. Nandi (2006), Satellite observations of CO and aerosol over Mexico City, *Atmos. Environ.*, *40*, 6019–6031, doi:10.1016/j.atmosenv.2005.11.065.

Novelli, P. C., L. P. Steele, and P. P. Tans (1992), Mixing ratios of carbon monoxide in the troposphere, *J. Geophys. Res.*, *97*, 20,731–20,750.

O'Neill, N., et al. (2008), Spectral deconvolution algorithm, Technical memo, Goddard Space Flight Cent., Greenbelt, Md.

Remer, L. A., et al. (2005), The MODIS aerosol algorithm, products and validation, *J. Atmos. Sci.*, *62*(4), 947–973, doi:10.1175/JAS3385.1.

Smirnov, A., B. N. Holben, T. F. Eck, O. Dubovik, and I. Slutsker (2000), Cloud screening and quality control algorithms for the AERONET database, *Remote Sens. Environ.*, *73*, 337–349, doi:10.1016/S0034-4257(00)00109-7.

Streets, D. G., Y. Wu, and M. Chin (2006), Two-decadal aerosol trends and a likely explanation of the global dimming/brightening transition, *Geophys. Res. Lett.*, *33*, L15806, doi:10.1029/2006GL026471.

Tanré, D., Y. J. Kaufman, M. Herman, and S. Mattoo (1997), Remote sensing of aerosol properties over oceans using the MODIS/EOS spectral radiances, *J. Geophys. Res.*, *102*, 16,971–16,988, doi:10.1029/96JD03437.

van der Werf, G. R., J. T. Randerson, L. Giglio, G. J. Collatz, P. S. Kasibhatla, and A. F. Arellano Jr. (2006), Interannual variability in global biomass burning emissions from 1997 to 2004, *Atmos. Chem. Phys.*, *6*, 3423–3441.

Yu, H., R. E. Dickinson, M. Chin, Y. J. Kaufman, B. N. Holben, I. V. Geogdzhayev, and M. I. Mishchenko (2003), Annual cycle of global distributions of aerosol optical depth from integration of MODIS retrievals and GOCART model simulations, *J. Geophys. Res.*, *108*(D3), 4128, doi:10.1029/2002JD002717.

H. Bian, M. Chin, T. Diehl, S. R. Kawa, T. Kucsera, and H. Yu, Laboratory for Atmospheres, NASA Goddard Space Flight Center, Greenbelt, MD 20771, USA. (huisheng.bian@nasa.gov)